

**ANTIBACTERIAL AND CELL INTERACTION OF TiO₂-BASED
NANOPARTICLES AND NANOTUBES**

by

NUR HIDAYATI BINTI AHMAD BARUDIN

**Thesis submitted in fulfillment of the
requirements for the degree of
Master of Science**

MARCH 2014

DECLARATION

I hereby declare that I have conducted, completed the research work and written the dissertation entitles “Antibacterial and Cell Interaction Studies of TiO₂-based Nanoparticles and Nanotubes” I also declare that it has not been previously submitted for the award of any degree or diploma or other similar title of this for any other examining body or university. This research data are confidential and therefore need to obtain supervisor approval to view or refer.

Name of student: NUR HIDAYATI BINTI AHMAD BARUDIN

Signature:

Date: 28 FEBRUARY 2014

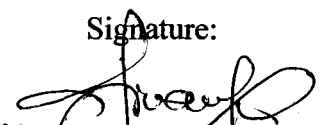


Witness by

Supervisor: ASSOC. PROF. DR. SRIMALA SREEKANTAN

Signature:

Date: 28 FEBRUARY 2014



Assoc. Prof. Engr. Dr. Srimala Sreekantan
B. Eng (Hons), M. Sc., Ph. D (USM)
Lecturer
School of Materials & Mineral Resources Engineering
Engineering Campus,
Universiti Sains Malaysia,
Seri Ampangan, 14300 Nibong Tebal,
Pcnang, Malaysia.
Email : srimala@eng.usm.my

ACKNOWLEDGEMENTS

First and foremost, I would like to express sincere thanks to my main supervisor Assoc. Prof. Dr Srimala Sreekantan for her guidance and continuous support throughout this study. I owe the warmest thanks to my co-supervisor, Dr Ong Ming Thong for his advice and support along antimicrobial testing study.

This work was carried out at the School of Materials and Mineral Resources Engineering, Universiti Sains Malaysia with cooperation with the Institute for Research in Molecular Medicine (INFORMM), Universiti Sains Malaysia. I would also like to thank the technicians and staffs in School of Materials and Mineral Resources Engineering and INFORMM for their cooperation and favors for helping all the testing involved. Next, I would like to thank all my friends in the nanomaterial group for their advice and suggestion in performing analysis to make this thesis possible.

I also want to express my deepest gratitude goes to my beloved parents (Ahmad Barudin Mohamad and Hasnah Ab Rahman) and my family for their support and encouragement over the years of my studies. My final and greatest debt is to my beloved husband, Mohd Fariz Mat Rahim who patiently took responsibility give unfailing support which made this thesis accomplish successfully. Thank you.

TABLE OF CONTENTS

ACKNOWLEDGEMENTS	ii
TABLE OF CONTENTS	iii
LIST OF TABLES	viii
LIST OF FIGURES	x
LIST OF ABBREVIATIONS	xv
LIST OF SYMBOLS	xvi
ABSTRAK	xvii
ABSTRACT	xix
CHAPTER 1	1
1.1 Introduction	1
1.2 Biological contaminants	1
1.3 Problem statement	3
1.4 Objectives	7
1.5 Scope of work	7
CHAPTER 2	9
2.1 Introduction	9
2.2 Indoor air pollution	9
2.3 Implant-related infections	10
2.4 Photocatalyst	10
2.4.1 Properties of TiO ₂	11
2.4.2 TiO ₂ nanoparticles	13
2.4.3 TiO ₂ nanotubes	15
2.4.4 Modification of TiO ₂ to harvest visible light	16

2.4.4.1	Noble metal loading	17
2.4.4.2	Metal ion loading	21
2.5	Photocatalytic inactivation of microorganism	24
2.6	Factors affecting the inactivation of bacteria and other microorganism	25
2.6.1	Wavelength and light intensity	25
2.6.2	Types of bacteria	26
2.6.3	Concentration of TiO ₂	28
2.6.4	Crystal structure and loading of TiO ₂	31
2.7	Synthesis of TiO ₂	32
2.7.1	Hydrothermal	32
2.7.2	Sol gel	35
2.7.3	Anodization	38
2.8	Application of TiO ₂	40
2.8.1	Air purification	41
2.8.2	Water application	42
2.8.3	Biomedical applications	43
2.9	Toxic effects of the interaction of TiO ₂	44
2.10	Standard methods for antibacterial activity	45
CHAPTER 3		46
3.0	Introduction	46
3.1	Raw materials selection	48
3.1.1	Raw materials to synthesis TiO ₂ nanosolution	48
3.1.2	Raw materials to synthesis TiO ₂ nanotubes	48
3.1.3	Raw materials for antibacterial activity	49
3.1.4	Raw materials for cell interaction	50
3.2	TiO ₂ nanoparticles	51

3.2.1	Synthesis of TiO ₂	52
3.2.2	Synthesis of Ag-TiO ₂	52
3.2.3	Synthesis of Zr-TiO ₂	53
3.2.4	Synthesis of Ag-Zr-TiO ₂	53
3.3	Formation of TiO ₂ nanotubes	54
3.3.1	Ti foil preparation	54
3.3.2	Electrolyte preparation	54
3.3.3	Anodization process	55
3.3.4	Cleaning of the as-anodized TiO ₂ foil	56
3.3.5	Heat treatment process	57
3.3.6	Wet impregnation	57
3.4	Characterization	58
3.4.1	Field Emission Scanning Electron Microscopy (FESEM)	58
3.4.2	X-Ray Diffraction (XRD)	59
3.4.3	Transmission Electron Microscopy (TEM)	60
3.4.4	Photoluminescence Spectroscopy (PL)	61
3.4.5	Raman Spectroscopy	62
3.4.6	X-ray Photoelectron Spectroscopy (XPS)	62
3.5	TiO ₂ nanoparticles antibacterial tests	63
3.5.1	Preparation of bacterial and fungal inoculums	63
3.5.2	Disc diffusion assay	64
3.5.3	Cotton diffusion assay (Embedded method)	64
3.5.4	Swab test	65
3.5.5	Cell morphology observation by TEM	66
3.5.6	Bacteria adhesion observation on sample surfaces by SEM	67
3.5.7	Colony count	68
3.5.8	Cytotoxicity test	69

3.6	TiO ₂ nanotubes antibacterial tests	70
3.6.1	Colony count	70
3.6.2	Cell interaction	71
3.6.3	Measurement of cell growth inhibition	72
3.6.4	Direct cytotoxicity tests on the nanotube	72
3.6.5	Statistical methods	73
CHAPTER 4		74
4.1	Introduction	74
4.2	Synthesis of TiO ₂	74
4.2.1	Hydrolysis and condensation process	74
4.2.2	Peptization process	75
4.2.3	TiO ₂ in optimized condition	76
4.3	Synthesis of Zr-TiO ₂	81
4.3.1	Effect of Zr concentration	82
4.4	Synthesis of Ag-TiO ₂	83
4.4.1	Effect of Ag concentration	84
4.5	Synthesis Ag-Zr-TiO ₂	95
4.5.1	Effect of Ag-Zr concentration	95
4.6	Antibacterial activity	102
4.6.1	Swab test	102
4.6.2	Minimum inhibitory concentration (MIC)	103
4.6.3	Colony count results	103
4.6.4	SEM microscopy of bacteria	105
4.6.5	Transmission electron microscopy of treated bacteria.	107
4.6.6	Toxicity test of TiO ₂ nanoparticles	113
4.7	TiO ₂ nanotubes	115

4.7.1	Morphology of Ti foil	115
4.7.2	Effects of different voltage	117
4.7.4	Wet impregnation	124
4.7.5	Antimicrobial activity of TiO ₂ nanotubes	126
4.7.6	Toxicity test	127
CHAPTER 5		132
5.1	Conclusions	132
5.2	Suggestions and recommendations	133
REFERENCES		134

LIST OF TABLES

		Page
Table 1.1	Summary on properties of each modified TiO ₂ .	6
Table 2.1	Physical and structural properties of anatase and rutile structure of TiO ₂ (Sherub <i>et al.</i> , 2008).	12
Table 2.2	Comparison of Gram-positive vs. Gram-negative bacteria cell walls (Wolf and Goldberg, 2006) (Umadevi <i>et al.</i>).	29
Table 2.3	Different concentration of TiO ₂ .	30
Table 2.4	Fundamental properties of rutile and anatase TiO ₂ (Sherub <i>et al.</i> , 2008).	31
Table 2.5	Summary of the works reported on the recent approach to synthesis TiO ₂ nanoparticles via hydrothermal technique.	34
Table 2.6	Summary of the works reported on the recent approach to synthesis nano-size TiO ₂ via sol-gel technique.	37
Table 2.7	Studies killing efficiency of TiO ₂ .	45
Table 3.1	List of raw materials and chemicals used to synthesis TiO ₂ nanosolution with its function and manufacturer.	48
Table 3.2	List of raw materials and chemicals used to synthesis TiO ₂ nanotubes with its function and manufacturer.	49
Table 3.3	List of raw materials and chemicals used for antibacterial activity with its function and manufacturer.	50
Table 3.4	List of raw materials for cell interaction testing.	51
Table 3.5	Amount of silver nitrate added.	52
Table 3.6	Amount of zirconium (IV) propoxide solution added.	53
Table 3.7	Composition of Ag-Zr-TiO ₂ .	53
Table 3.8	Constant parameters used in anodization process to produce TiO ₂ nanotubes.	56
Table 4.1	Zones of inhibition measured (in mm) from disc diffusion assay.	83
Table 4.2	Zones of inhibition measured (in mm) from cotton diffusion assay.	86
Table 4.3	Zone of inhibition of Ag-Zr-TiO ₂ .	96

LIST OF FIGURES

		Page
Figure 1.1	Flow chart of the project.	8
Figure 2.1	Mechanism of TiO ₂ photocatalysis: $h\nu_1$: pure TiO ₂ ; $h\nu_2$: metal-doped TiO ₂ and $h\nu_3$: nonmetal-doped TiO ₂ .	18
Figure 2.2	Effect of cationic doping compounds in terms of visible light absorbance and photocatalytic activity (Hwang <i>et al.</i> , 2006, Yanjun <i>et al.</i> , 2006).	21
Figure 2.3	Photocatalytic inactivation of microorganisms.	25
Figure 2.4	(a) Gram-positive cell wall and (b) Gram-negative cell wall (Wolf and Goldberg, 2006).	27
Figure 2.5	Crystal structures of (a) rutile and (b) anatase of TiO ₂ (Moellmann <i>et al.</i> , 2012)	31
Figure 2.6	Schematic set-up for anodization experiments.	39
Figure 2.7	Illustrative top and cross sectional FESEM images of TiO ₂ nanotubes arrays synthesis by anodization of Ti films (Xiao, 2012).	39
Figure 2.8	Schematic diagram (left column) and SEM sequence (top-views – middle column, cross-sections – right column) of different stages of the TiO ₂ nanotubes layer formation.	40
Figure 3.1	Flow chart of stage 1.	46
Figure 3.2	Flow chart of stage 2.	47
Figure 3.3	Flow chart of stage 3.	47
Figure 3.4	Schematic diagram of experiment setup for anodization process (Lai <i>et al.</i> , 2012).	55
Figure 3.5	Annealing profile for crystallization of TiO ₂ nanotubes.	57
Figure 3.6	Basic working principle of XRD (Warren, 1969).	60
Figure 3.7	Flowchart of embedded method methodology.	65
Figure 3.8	Flowchart of colony count methodology for TiO ₂ nanoparticles.	68

Figure 3.9	Flowchart of colony count methodology for TiO ₂ nanotubes.	71
Figure 4.1	XRD pattern of TiO ₂ .	76
Figure 4.2	Raman spectra of TiO ₂ .	77
Figure 4.3	TEM image of TiO ₂ .	77
Figure 4.4	Photoluminescence spectra of TiO ₂ .	78
Figure 4.5	XPS survey spectra for TiO ₂ .	79
Figure 4.6	XPS spectrum of Ti2p of TiO ₂ .	80
Figure 4.7	XPS spectrum of C1s of TiO ₂ .	80
Figure 4.8	XPS spectrum of O1s of TiO ₂ .	81
Figure 4.9	Inhibition zone of Zr-TiO ₂ .	82
Figure 4.10	Images results for (a) 1% Zr-TiO ₂ , (b) 2% Zr-TiO ₂ , (c) 3% Zr-TiO ₂ and (d) 4% Zr-TiO ₂ versus <i>E. coli</i> for 24 hours.	83
Figure 4.11	Images results for (a) 1% Zr-TiO ₂ , (b) 2% Zr-TiO ₂ , (c) 3% Zr-TiO ₂ and (d) 4% Zr-TiO ₂ versus <i>S. aureus</i> for 24 hours.	83
Figure 4.12	Inhibition zone of <i>E. coli</i> upon different Ag concentration (a) control (HNO ₃), (b) positive control (Ag alone) (c) TiO ₂ , (d) 0.1, (e) 0.3, (f) 0.5, (g) 0.7, and (h) 0.9 g Ag-TiO ₂ .	85
Figure 4.13	Inhibition zone of <i>A. niger</i> upon Ag concentration (a) control (HNO ₃), (b) positive control (Ag alone) (c) TiO ₂ , (d) 0.1, (e) 0.3, (f) 0.5, (g) 0.7, and (h) 0.9 g Ag-TiO ₂ .	86
Figure 4.14	Inhibition zone of 0.1 Ag-TiO ₂ .	87
Figure 4.15	Inhibition zone of (a) TiO ₂ , (b) <i>E. coli</i> and (c) <i>S. aureus</i> for 0.1 Ag-TiO ₂ .	87
Figure 4.16	XRD pattern of (a) TiO ₂ and Ag-TiO ₂ .	88
Figure 4.17	TEM images of Ag-TiO ₂ .	88
Figure 4.18	Raman spectra of (a) TiO ₂ and (b) Ag-TiO ₂ .	89
Figure 4.19	Photoluminescence (PL) spectra of (a) TiO ₂ and (b) Ag-TiO ₂ .	90
Figure 4.20	XPS survey spectra for Ag-TiO ₂ .	91

Figure 4.21	XPS spectra of Ti2p of Ag-TiO ₂ .	92
Figure 4.22	XPS spectra of Ag3d of Ag-TiO ₂ .	93
Figure 4.23	XPS spectra of O1s of Ag-TiO ₂ .	94
Figure 4.24	XPS spectra of O1s of TiO ₂ and Ag-TiO ₂ .	94
Figure 4.25	Inhibition zone of Ag-Zr-TiO ₂ .	95
Figure 4.26	Image results for (a) Ag-1% Zr-TiO ₂ (b) Ag-2% Zr-TiO ₂ (c) Ag-3% Zr-TiO ₂ (d) Ag-4% Zr-TiO ₂ versus <i>E. coli</i> for 24 hours.	96
Figure 4.27	Image results for (a) Ag-1% Zr-TiO ₂ (b) Ag-2% Zr-TiO ₂ (c) Ag-3% Zr-TiO ₂ (d) Ag-4% Zr-TiO ₂ versus <i>S. aureus</i> for 24 hours.	96
Figure 4.28	XRD patterns of (a) Ag-TiO ₂ and (b) Ag-4%Zr-TiO ₂ .	97
Figure 4.29	Raman spectra of (a) Ag-TiO ₂ and (b) Ag-4%Zr-TiO ₂ .	98
Figure 4.30	TEM images of Ag-4% Zr-TiO ₂ .	98
Figure 4.31	Photoluminescence (PL) spectra of (a) Ag-TiO ₂ and (b) Ag-4% Zr-TiO ₂ nanoparticles.	99
Figure 4.32	XPS wide spectrum of Ag-4% Zr-TiO ₂ nanoparticle.	100
Figure 4.33	XPS spectra of Zr 3d of Ag-4% Zr-TiO ₂ .	101
Figure 4.34	XPS spectra of Ag3d _{3/5} of Ag-4% Zr-TiO ₂ .	101
Figure 4.35	The antibacterial activities of Ag-TiO ₂ against bacteria <i>E. coli</i> at concentration (a) 0.2, (b) 0.1, (c) 0.05, and (d) 0.025 M.	103
Figure 4.36	Comparison of the survival bacteria (cells/ml) for the six different strains against 0.05 M of Ag-TiO ₂ .	104
Figure 4.37	SEM of microbial morphology of Gram-negative. (a) untreated <i>E. coli</i> , (b) treated <i>E. coli</i> , (c) untreated <i>P. aureginosa</i> and (d) treated <i>P. aureginosa</i> with Ag-TiO ₂ on glass slide.	105
Figure 4.38	SEM of microbial morphology of Gram-positive. (a) untreated <i>B. cereus</i> , (b) treated <i>B. cereus</i> , (c) untreated <i>B. subtilis</i> and (d) treated <i>B. subtilis</i> with Ag-TiO ₂ on glass slide.	106

Figure 4.39	Transmission electron micrographs of: (a) untreated, (b) 6 hours and (c) 12 hours treated with Ag-TiO ₂ against <i>E. coli</i> bacteria.	109
Figure 4.40	Transmission electron micrographs of: (a) untreated, (b) 6 hours and (c) 12 hours treated with Ag-TiO ₂ against <i>B. cereus</i> .	110
Figure 4.41	Schematic diagram illustrating the mechanism of Ag-TiO ₂ inactivate the microorganisms.	112
Figure 4.42	Effect of CCD-18Co cell line after 48 hour treatment with: (a) media, (b) 25 % phenol sample, (c) TiO ₂ , (d) Ag-TiO ₂ nanoparticles and (e) control.	114
Figure 4.43	% inhibition of cell proliferation (IC ₅₀) after treatment with various concentrations of TiO ₂ , Ag-TiO ₂ and control sample for 48 hours.	115
Figure 4.44	FESEM image showing the substrate of Ti. The inset reveals the morphology with high magnification.	116
Figure 4.45	EDX spectrum of pure Ti	116
Figure 4.46	FESEM images of TiO ₂ nanotubes obtained in ethylene glycol containing 5 wt % NH ₄ F and 5 ml H ₂ O ₂ for 60 minutes: (a) 20 V; (b) 40 V; and (c) 60 V.	118
Figure 4.47	Current density against time plot for anodized Ti foils at 40 V for 60 min in ethylene glycol electrolyte containing 5 wt % NH ₄ F and 5 wt % H ₂ O ₂ .	119
Figure 4.48	Top view and cross sectional view of FESEM images of TiO ₂ nanotubes using different 1 wt % of H ₂ O ₂ in ethylene glycol containing 5 wt % NH ₄ F for 1 hour at 60 V.	120
Figure 4.49	Top view and cross sectional view of FESEM images of TiO ₂ nanotubes using different 5 wt % of H ₂ O ₂ in ethylene glycol containing 5 wt % NH ₄ F for 1 hour at 60 V.	121
Figure 4.50	XRD patterns of TiO ₂ nanotube arrays (a) as anodized and (b) annealed 400 °C.	123
Figure 4.51	EDX spectrum of TiO ₂ nanotube arrays (a) as anodized and (b) annealed 400 °C.	123
Figure 4.52	EDX analysis of Ag-TiO ₂ nanotubes at spot A.	125
Figure 4.53	EDX elemental composition for Ag-TiO ₂ nanotubes.	125

Figure 4.54	XRD patterns of Ag-TiO ₂ nanotube arrays.	126
Figure 4.55	Antimicrobial activity test 1 against <i>E. coli</i> . Error bars indicate standard deviation (n=3).	127
Figure 4.56	Effect of direct contact of (a) HDP, (b) Ti, (c) TiO ₂ , (d) Ag-TiO ₂ and (e) PU on hFOB 1.19 cells after 24 and 48 hours.	130
Figure 4.57	The cell viability of hFOB 1.19 cell lines (Values are mean ± SD, n=3); *p<0.05 as compared to the controls.	131

LIST OF ABBREVIATIONS

TiO ₂	Titanium dioxide
TTIP	Titanium (IV) Isopropoxide
XRD	X-Ray Diffraction
SEM	Scanning Electron Microscopy
TEM	Transmission Electron Microscope
PL	Photoluminescence Spectroscopy
XPS	X-ray photoelectron Spectroscopy
MHA	Mueller Hinton Agar
MHB	Mueller Hinton Broth
MTS	Cell Titer 96 Aqueous Non- Radioactive Cell Proliferation Assay
DMEM	Ham's F12 Medium Dulbecco's Modified Eagle Medium
<i>E. coli</i>	Escherichia coli
<i>S. aureus</i>	Staphylococcus aureus
<i>B. subtilis</i>	Bacillus subtilis
ROS	Reactive oxygen species
UV	Ultraviolet

LIST OF SYMBOLS

Ag	Silver
Zr	Zirconium
HNO ₃	Nitric acid
AgNO ₃	Silver Nitrate
<i>hν</i>	Photon energy
<i>e</i> ⁻	Electron
<i>h</i>	Hole
HO ₂ [•]	Hydrogen superoxide radical
H ₂ O ₂	Hydrogen peroxide
ZrO ₂	Zirconium oxide
O ₂ ^{•-}	Superoxide radical anion
OH [•]	hydroxyl radical

KAJIAN ANTIBAKTERIA DAN TINDAK BALAS SEL TERHADAP NANOPARTIKEL DAN TIUB NANO TiO₂

ABSTRAK

Pada masa ini, sebahagian daripada masalah terbesar yang menjejaskan keseluruhan dunia adalah pencemaran udara dan juga mikrob bahan cemar. Setiap kali kita bernafas, kita mempertaruhkan kehidupan kita dengan menyedut bahan kimia berbahaya dan bahan cemar biologi yang telah merebak dengan cara mereka ke udara. Oleh itu dalam kerja-kerja ini, penggunaan bahan TiO₂ fotomangkin untuk mengatasi pencemar udara dalaman telah dikaji. Larutan-nano TiO₂ telah disediakan menggunakan kaedah sol-gel diikuti dengan proses peptitasi pada 85 °C selama 8 jam. Larutan-nano TiO₂ dengan saiz zarah 3-6 nm dengan struktur *anatase* telah dihasilkan. TiO₂ sahaja didapati tidak begitu berkesan dalam menunjukkan ciri-ciri antimikrobial. Oleh itu, kesan perak (Ag), zirkonium (Zr) dan perak- zirkonium (Ag-Zr) pada ciri-ciri antibakteria TiO₂ di bawah cahaya pendarfluor telah dikaji. Kiraan koloni selepas dirawat dengan 0.1 Ag- TiO₂ telah menunjukkan keupayaan bahan ini untuk membunuh bakteria lebih daripada 99.99 %. Kuasa pembunuhan merosot dalam urutan yang berikut: Ag-TiO₂ > Ag-Zr-TiO₂ > Zr-TiO₂ > TiO₂. Pemerhatian TEM dan SEM menunjukkan bahawa bakteria Gram-positif telah mudah reput berbanding dengan bakteria Gram-negatif. Nanopartikel Ag- TiO₂ menunjukkan kesan tidak toksik terhadap CCD-18Co bahagian sel fibroblast. Selain daripada TiO₂ dalam bentuk nanopartikel, kerja kajian telah dilanjutkan kepada struktur nanotubular. Tatasusunan TiO₂ tiub nano telah dibentuk oleh kaedah penganodan dengan voltan berbeza-beza dari 20, 40 dan 60 V. Diameter lebih besar dan tiub nano lebih panjang kemudiannya diresap ke dalam larutan perak untuk membentuk tiub nano Ag- TiO₂. Ujian aktiviti antimikrob terhadap *E. coli* menunjukkan bahawa permukaan tiub nano Ag-TiO₂ berkurangan 95.7 %

bakteria lekatan berbanding TiO_2 tulen. Dalam kajian vitro menunjukkan bahawa perak yang telah dimuatkan ke dalam tiub nano TiO_2 tidak toksik untuk sel hFOB 1.19.

ANTIBACTERIAL AND CELL INTERACTION OF TiO₂ BASED NANOPARTICLES AND NANOTUBES

ABSTRACT

Currently, some of the major problems affecting the world are air pollution as well as microbial contamination. Every time we breathe, we are risking our lives by inhaling dangerous chemicals and biological contaminants that have found their way into the air. In this work, the use of TiO₂ photocatalyst materials to overcome indoor air pollutants is investigated. The TiO₂ nanosolution was prepared by using sol-gel method followed by the peptization process at 85 °C for 8 hours. TiO₂ nanosolution with a particle size of 3-6 nm with an anatase structure was produced. TiO₂ alone was found to be not very effective in demonstrating the antimicrobial property. Therefore, the effect of silver (Ag), zirconium (Zr) and silver-zirconium (Ag-Zr) on antibacterial properties of TiO₂ under fluorescent light was studied. The colony count of the agar with 0.1 Ag-TiO₂ has indicated the capability of this material to kill bacteria by more than 99.99%. The killing power deteriorated in the following order: Ag-TiO₂ > Ag-Zr-TiO₂ > Zr-TiO₂ > TiO₂. TEM and SEM observations showed that the Gram-positive bacteria were easily decomposed compared to the Gram-negative bacteria. Ag-TiO₂ nanoparticles showed a non-toxic effect towards CCD-18Co fibroblast cell lines. Apart from TiO₂ in nanoparticle form, the work was extended to the nanotubular structure. TiO₂ nanotube arrays were formed by the anodization method with a voltage which varied from 20, 40 and 60 V. Larger diameters and longer nanotubes were then impregnated in the silver solution to form Ag-TiO₂ nanotubes. An antimicrobial activity test against *E. coli* demonstrated that the Ag-TiO₂ nanotube surface significantly reduced 95.7 % of bacteria adhesion as compared to pure TiO₂. The *in vitro* study showed that the silver loaded TiO₂ nanotubes were not cytotoxic for hFOB 1.19 cells.

CHAPTER 1

INTRODUCTION

1.1 Introduction

This research was conducted to evaluate the antibacterial property and the toxicity of TiO₂ nanoparticles and nanotubes. TiO₂ nanoparticles were synthesized using the sol gel process and TiO₂ nanotubes were produced using the anodization method. The synthesis of TiO₂, Zr incorporated TiO₂ (Zr-TiO₂), Ag incorporated TiO₂ (Ag-TiO₂) and silver-zirconium (Ag-Zr) incorporated TiO₂ (Ag-Zr-TiO₂) nanoparticles were produced using the sol gel method. This process was performed to produce a milky white colloid TiO₂ followed by peptization to disperse the white colloid into nano sized particles (3-6 nm). The optimization process was carried out by studying the performance efficiency of the antibacterial activity. From these synthesized nanoparticles, Ag-TiO₂ with an optimum formulation was selected to be loaded in nanotubular form using the wet impregnation process. The antimicrobial activity and the toxicity of TiO₂ nanoparticles and nanotubes were investigated. The presence of cation loading (Ag or Zr) in TiO₂ is believed to induce a photocatalytic property that can yield high reactivity under fluorescent light that leads to pathogenic bacteria deactivation.

1.2 Biological contaminants

Microorganisms are believed to have existed billions of years ago and they give a large contribution to the world ecosystem. Microorganisms such as photosynthetic bacteria consume carbon dioxide and produce oxygen, sustaining the oxygen composition in the atmosphere. However, there are some groups of microorganisms such as *E. coli*, *S. aureus*, *B. cereus*, *A. niger* and other pathogenic bacteria that are

infectious and can cause diseases. According to the fact sheet updated by the World Health Organization (WHO) in 2011, 2 million out of 59 million premature deaths each year are attributed to polluted indoor air. In tropical countries like Singapore and Malaysia, warm and humid climate aggravates the growth of indoor biological contaminants. The use of air conditioners, humidifiers and unvented heaters increases moisture over interior surfaces (EPA, 1995). Hence, this encourages the growth of biological pollutions such as allergens and may cause asthma, cough, mumps, rubella, pneumonia and influenza (Jacoby *et al.*, 1998). Moreover, more than 60 bacteria, viruses and fungi are documented as infectious airborne pathogens (Jacoby *et al.*, 1998). Hence, the control of indoor air quality through economical and effective inactivation of microorganisms is required.

In addition, bacterial infection is also known as a common problem after orthopedic implant surgery. In USA, 1%–1.5% of all total hip and knee arthroplasties (THAs and TKAs, respectively) implantations suffer from the risk of infection (Stanton, 2010). Although the chance of infection is rare in these procedures, the problem is significant as periprosthetic implant infections cost about US\$70,000 per episode and is the most common cause of revision surgery in all TKAs (25%), the third commonest cause in all THAs (15%), and the commonest reason for the removal of all TKAs (79%) and THAs (74%) (Stanton, 2010, Bozic *et al.*, 2010, Bozic *et al.*, 2009). If not prevented, bacterial infection can result in serious and life threatening conditions such as osteomyelitis and implant loosening (Popat *et al.*, 2007a). Acute infection or chronic osteomyelitis develops in as many as 5%–33% of implant surgeries despite the use of strict antiseptic operative procedures (Hendriks *et al.*, 2004).

1.3 Problem statement

Several methods have been used to kill bacteria. Many control methods are used to reduce indoor bio-pollutants through purging (using outside air), filtering and isolating microbiological species using pressurization control and ultraviolet germicidal irradiation (UVGI). The recommendation of introducing outside air to purge the contaminant indoors only dilute the concentration of microorganisms without destroying the biological species (ASHRAE, 1997). Pressurization control is commonly used in biohazard facilities and isolation rooms to prevent the migration of microbes from one area to another but inherent costs and operational instability at normal air flow rates limit its applications for common indoor environments (e.g., residential buildings) (Kowalski and Bahnfleth, 1998).

Controlled antibiotics released from biomaterials can prevent microbial infection but there is concern about microbial resistance to antibiotics including *S. aureus* and *S. epidermis* (Puckett *et al.*, 2010). The prevention of bacteria adhesion without antibiotics is one of the best ways to reduce orthopedic implant application. Ultraviolet (UV) radiation has received great attention to reduce indoor bio-pollutants and prevent biomaterial-related infections. UV disinfection can inactivate protozoa, bacteria and viruses (Hijnen *et al.*, 2006). UV may impair bacterial adhesion in implant application but will not compromise the good response of human bone-forming cells to implant (Gallardo-Moreno *et al.*, 2009). Although UV radiation shows the highest efficiency in killing microorganisms, its adverse effects to the human body is critical and inevitable (Zhang and Sun, 2004). The short-term over exposure of human skin and eyes to 254 nm UV-C can lead to erythema or reddening of the skin, photokeratitis/inflammation of

the cornea and conjunctivitis/inflammation of the conjunctiva (Green and Scarpino, 2002).

TiO₂ photocatalysis is capable of inactivating microbial toxins (e.g. lipopolysaccharide endotoxin, brevetoxins, microcystins) but only under UV irradiation (Foster *et al.*, 2011) as shown in Table 1.1. The bactericidal efficiency of photocatalysis using UV and TiO₂ has also been tested in the treatment of pathogenic microbes including bacteria, fungi, viruses and cancer cells (Sunada *et al.*, 2003, Rincón and Pulgarin, 2003, Foster *et al.*, 2011, Rahim *et al.*, 2012) but the use of ultraviolet for effective photocatalysis gives adverse effects to the human body (Prasad *et al.*, 2009, Wu *et al.*, 2010). Using fluorescent light can be an attractive and alternative light source since indoor environments, especially hospitals and office premises, are commonly illuminated using fluorescent light. TiO₂ coupled with fluorescent light has a vast potential for indoor air disinfection due to low power consumption, less frequent maintenance requirement and compatibility with the heating ventilation system (Yang and Wang, 2008).

TiO₂ is incorporated with other metals so that it can detoxify microorganisms under fluorescent light effectively. Ag is selected because silver in ionic or nanoparticle form has a high antimicrobial activity thus, it can enhance the charge separation efficiently. Its Fermi level is lower than TiO₂ which results in imposing empty states in between the bandgap. More importantly, Ag is an antibacterial agent by nature (Baker *et al.*, 2005). Most studies reported on the toxicity of TiO₂ nanoparticles but not many study focussed on the toxicity of Ag-TiO₂.

Zr has the potential to deactivate bacteria because many reports have shown that Zr-doped titanium solid solutions can enhance photocatalytic activity in visible light. Zr is selected because it has a slightly greater ionic size than Ti^{4+} . Zr will substitute Ti^{4+} inducing lattice strain which later forces the oxygen to escape from its lattice giving an empty state to prolong the recombination lifetime. Zr-TiO₂ has the potential to kill bacteria but only under sunlight (Green and Scarpino, 2002). The antibacterial strength of Zr incorporated TiO₂ nanoparticles under fluorescent light has not been widely studied. Therefore, the effect of increasing the amount of Zr on antibacterial strength will be studied. For Ag-Zr-TiO₂ composition, only one work has been reported (Moafi *et al.*, 2011). However, it only focused on the performance of photocatalytic activity, not the antibacterial properties. Interestingly, there no work on the toxicity of Ag-Zr-TiO₂ has been reported. Table 1.1 shows the reports on the photocatalytic, antibacterial and toxicity studies of each modified TiO₂.

TiO₂ nanoparticles are still far from becoming a potential candidate for bactericidal application due to the effects of toxicity problems. Some reports have found that TiO₂ nanoparticles are toxic to human health (Oberdörster *et al.*, 1994, Oberdörster, 2000, Zhao *et al.*, 2009, Zhao and Castranova, 2011). However, there are claim that TiO₂ is not toxic (Karlsson *et al.*, 2008, Ramires *et al.*, 2001). Dechsakulthorn *et al.* (2007) have shown the toxic effects of TiO₂ NP to human skin fibroblasts during 24 hours exposure to NPs of less than 150 nm diameter. Similarly Peter *et al.* (2004), Kang *et al.* (2011) and Yin *et al.* (2012) have shown the toxic effects for nanoparticles that are less than 100 nm in size. Gurr *et al.* (2005) reported that TiO₂ nanoparticles that are less than 200 nm were not claimed as toxic compared to nanoparticles which had diameters

of 10-20 nm. Research has shown that smaller nanoparticles may exert a higher degree of toxicity (Hund-Rink and Simon 2006; Franklin et al., 2007).

Table 1.1 Summary on the properties of each modified TiO₂.

Studies	TiO ₂	Ag-TiO ₂	Zr-TiO ₂	Ag-Zr-TiO ₂
Photocatalyst	Good under UV light (Prasad <i>et al.</i> , 2009, Kim <i>et al.</i> , 2008b, Markowska-Szczupak <i>et al.</i> , 2011)	Improve photocatalytic activity under visible light. (Hou <i>et al.</i> , 2009, Grandcolas <i>et al.</i> , 2011, Ashkarran <i>et al.</i> , 2011)	Good photocatalyst under visible light (Stengl <i>et al.</i> , 2008, Ragai and Yacoub, 2013, Moafi <i>et al.</i> , 2011)	Very good photocatalyst under visible light (Moafi <i>et al.</i> , 2011)
Antibacterial	Good under UV light (Amin <i>et al.</i> , 2009, Swetha <i>et al.</i> , 2010b, Foster <i>et al.</i> , 2011)	Excellent antibacterial strength under visible light (Grandcolas <i>et al.</i> , 2011, Ashkarran <i>et al.</i> , 2011, Gupta <i>et al.</i> , 2013)	Good bacterial strength under sunlight (Green and Scarpino, 2002) No reported under visible light.	Not reported
Toxicity	Toxic if size less 100 nm (Dechsakulthorn <i>et al.</i> , 2007, Kang <i>et al.</i> , 2011, Yin <i>et al.</i> , 2012)	Can kill HeLa cells (cancer cell) by 100% (Jacoby <i>et al.</i> , 1998)	Not reported	Not reported

The objective of this research is to improve the antibacterial properties of TiO₂ nanoparticles and nanotubes that can kill bacteria at a faster killing rate than what has been reported in previous works. In addition, the utilization of TiO₂ nanoparticles with the size of less than 6 nm must be proven to be harmless to human bodies. Therefore, this study is also coupled with a toxicity test to investigate TiO₂ nanoparticles and nanotubes that do not have undesirable side effects to human health.

1.4 Objectives

- i. To synthesize TiO_2 , Zr-TiO_2 , Ag-TiO_2 , and Ag-Zr-TiO_2 nanoparticles using the sol gel method.
- ii. To study the formation of TiO_2 nanotubes via anodization followed by the wet impregnation method to form doped-nanotubes from the optimized formulation in objective (i).
- iii. To investigate the antibacterial activity and toxicity of cation- TiO_2 nanoparticles and nanotubes under fluorescent light.

1.5 Scope of work

This project is divided into two categories in order to achieve the objectives. The first is the TiO_2 nanoparticles and the second part is the TiO_2 nanotubes. TiO_2 nanoparticles were synthesized using the sol gel approach based on a preliminary study (Ibrahim and Sreekantan, 2010). Zr-TiO_2 , Ag-TiO_2 , and Ag-Zr-TiO_2 were also synthesized. The optimization process was carried out by studying the performance efficiency of the antibacterial activity of Ag and Zr that were incorporated into TiO_2 under fluorescent light. The structural and optical properties of the best optimized samples were characterized using PL, RAMAN, XPS, XRD, TEM and SEM. The sample was then selected to the study of the toxicity test. TiO_2 nanotubes were synthesized using the anodization method to obtain get highly ordered TiO_2 nanostructures. A set of experiments was conducted by adapting the optimum condition and controlled dimensional features for TiO_2 nanotubes formation based on preliminary studies (Lai *et al.*, 2012). From these synthesized nanoparticles, Ag-TiO_2 with the optimum formulation was selected to be loaded in nanotubular form. Antimicrobial activity test against *E. coli* was conducted. The structural properties were characterized

using XRD, EDX, and SEM analysis. The toxicity study of the silver loaded nanotubes was also investigated; it was found that they are safe to be used on human beings. The project overview is summarized in Figure 1.1.

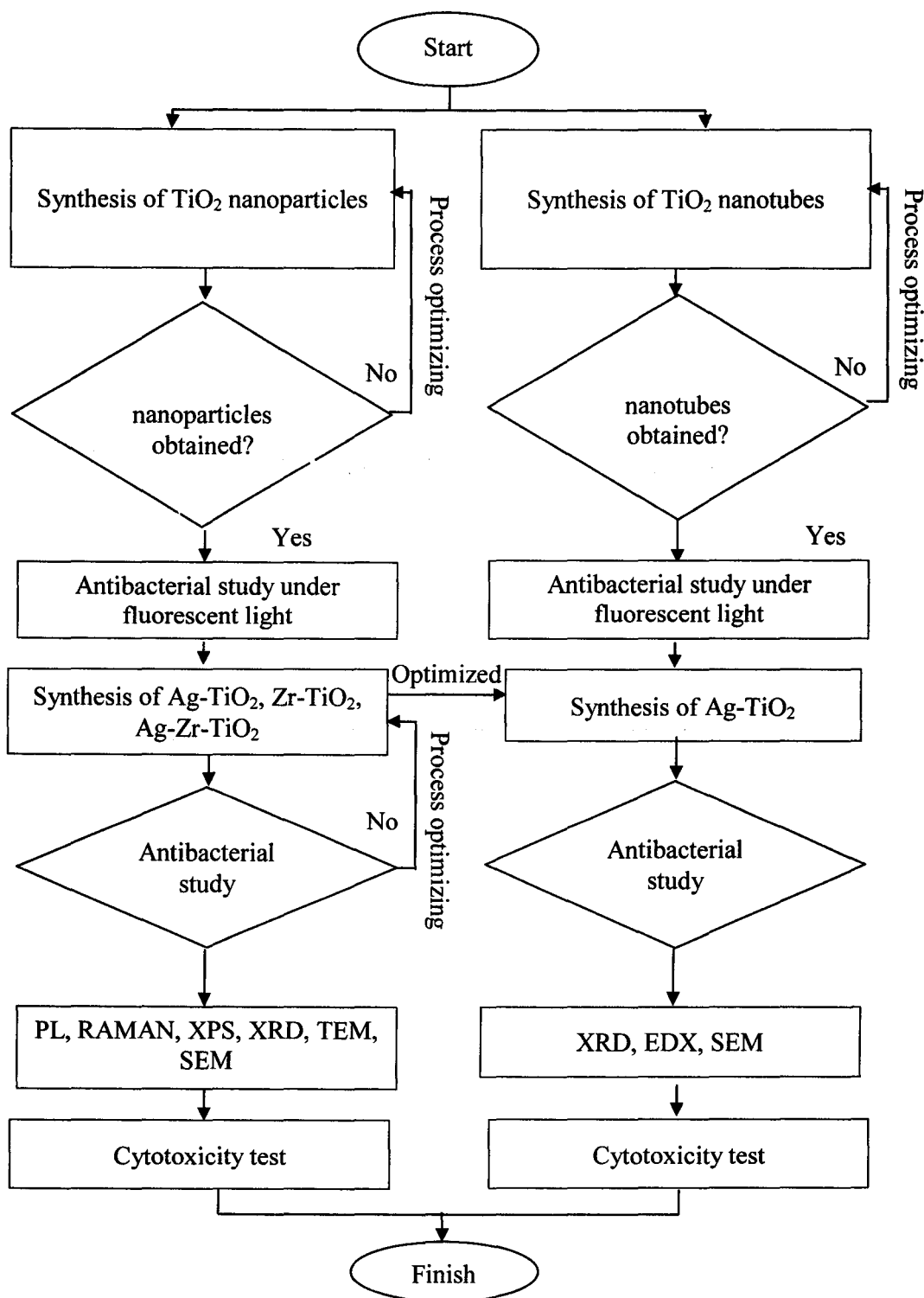


Figure 1.1: Flow chart of the project.

CHAPTER 2

LITERATURE REVIEW

2.1 Introduction

This chapter covers two main topics; the first is on TiO₂ nanoparticles and the second is on TiO₂ nanotubes. TiO₂ nanoparticles are used for indoor air quality problems and TiO₂ nanotubes are used for implant applications. The properties of TiO₂ nanoparticles and nanotubes that are related to photocatalytic activity and bacterial effects are discussed in this chapter. The toxicity effects are also evaluated.

2.2 Indoor air pollution

Indoor air pollution is recognized as a public health problem as most people spend 80%-90% of their time indoors and in enclosed work areas (Society, 1990). According to research, each individual inhales about 20,000 liters of air every day. Every time we breathe, we are risking our lives by inhaling dangerous chemicals and biological contaminants that have found their way into the air. Microorganisms are responsible for irritant responses, infectious diseases, respiratory problems and hypersensitive reactions (Green and Scarpino, 2002). Furthermore, the contamination of indoor air by microbial pollutants may be responsible for the sick-building syndrome (SBS) and the building-related syndrome (BRI) (Bholah and Subratty, 2002). For example, airborne transmission of *Mycobacterium tuberculosis* and other infectious agents in the indoor environments are hazardous (Xu *et al.*, 2003). As the world becomes industrialized and its population grows rapidly, the aforementioned problems have intensified. Since indoor air pollution is one of the top five environmental risks

(USEPA, 1995), the economical and effective prevention of disease spreading microorganisms indoors are needed.

2.3 Implant-related infections

According to the Canadian Joint Replacement Registry (CJRR) 2008-2009 annual report, the number of hospitalizations for hip and knee replacement has been increasing steadily in the past 10 years (CJRR, 2009). In USA, it was estimated that the number of annual primary total knee replacements would increase from 450,400 in 2005 to 3.48 million by 2030, compared with the growth of the annual primary total hip replacements from 208,600 in 2005 to 572,100 by 2030 (American Academy of Orthopaedic Surgeons). After surgery, various complications occur such as dislocation, loosening and prosthetic-related infections. Despite considerable progress in the prevention and the treatment of implant-associated infections, the number of patients with such infections is rising due to the lifelong risk of bacterial seeding on the implant (Trampuz and Widmer, 2006). Widmer *et al.* (2001) has reported that the infection rates after revision surgery are usually higher (5%-40%) than after primary replacement. Due to the rise of the percentage of patients aged over 65 years in industrialized countries, the number of patients requiring implants will continue to grow, as well as the risk for orthopedic device-related infections (ODRIs) (Widmer, 2001). Considering the huge population of patients with orthopedic implants and the serious consequences, this problem should not be underestimated.

2.4 Photocatalyst

In 1995, the photocatalyst was discovered in Japan. When a photocatalyst material is exposed to light, it absorbs photon energy and causes various chemical

reactions. In recent years, semiconductor photocatalysis has emerged as one of the most promising technologies because it represents an easy way to utilize the energy of either natural sunlight or artificial indoor illumination and is abundantly available everywhere in the world (Jiang *et al.*, 2012). The potential applications of photocatalysis are found mainly in the following fields: (i) photolysis of water to yield hydrogen fuel; (ii) photodecomposition or photooxidization of hazardous substances; (iii) artificial photosynthesis; (iv) photoinduced superhydrophilicity; and (v) photoelectrochemical conversion (Tong *et al.*, 2012). Various n-type semiconductor metal oxides such as TiO₂, ZnO, CdS and SnO₂ have been tested for the photocatalytic oxidation of organic pollutants in water and air. Zinc oxide self-deactivates by forming Zn²⁺ ions when it reacts with photogenerated holes in the water which can dissolve into the solution (Kuo and Shueh, 2003, Jung *et al.*, 2005). CdS also showed the same photocorrosion effect in solution by releasing toxic Cd²⁺ ions in an aqueous media (Kuo and Shueh, 2003, Zhang *et al.*, 2006). Tin oxide has a wider band gap of 3.5-4.2 eV (350-300 nm), which utilizes a lesser fraction of UV light and thus, has a lower relative photoactivity (Koumoto *et al.*, 1999). Among the semiconductors reported, TiO₂ has generally exhibited the highest photocatalytic activity in a wider range of environmental applications. TiO₂ offers great promise for indoor air purification and has a positive impact on biomedical applications (Hyun Kim *et al.*, 2006, Popat *et al.*, 2007b). Therefore, TiO₂ was chosen to be used in this research.

2.4.1 Properties of TiO₂

TiO₂ is a semiconductor with high photochemical stability, low cost, good photoactivity, and nontoxicity (Kment *et al.*, 2010, Markowska-Szczupak *et al.*, 2011). It is chemically inert and thermally stable, non-flammable and non-toxic. Bioactivity

has become a desired property of TiO₂ in the development of biomaterials (Brohede *et al.*, 2009, Piskounova *et al.*, 2009, Forsgren *et al.*, 2011). Titanium metals and alloys, with the anatase phase, have good bioactive properties (Kokubo, 1996, Forsgren *et al.*, 2007, Brohede *et al.*, 2009, Grigal *et al.*, 2012). Titanium is one of the few biocompatible metals which can osseointegrate. Moreover, TiO₂ is reputed to be toxic to both Gram-negative and Gram-positive bacteria (Adams *et al.*, 2006). Table 2.1 shows some of the physical and structural properties of TiO₂. TiO₂ exists in three different phases: anatase, rutile and brookite.

Table 2.1: Physical and structural properties of anatase and rutile structure of TiO₂ (Sherub *et al.*, 2008).

Property	Anatase	Rutile
Molecular weight (g/mol)	79.88	79.88
Melting point (°C)	1825	1825
Boiling point (°C)	2500-3000	2500-3000
Specific gravity	3.9	4.0
Light absorption (nm)	$\lambda \leq 385$ nm	$\lambda \leq 415$ nm
Mohr's Hardness	5.5	6.5 to 7
Refractive index	2.55	2.75
Dielectric constant	31	114
Crystal structure	Tetragonal	Tetragonal
Lattice Constants(A°)	a= 3.784 c= 9.515	a= 4.5936 c= 2.9587
Density (g/cm ³)	3.79	4.13
Ti-O bond length (A°)	1.937 (4) 1.965 (2)	1.949 (4) 1.980 (2)

Electronic properties such as band gap play an important role in the photocatalyst performance. The anatase phase of TiO₂ has a higher band gap (3.2 eV) compared to rutile (3.0 eV) and brookite. Anatase TiO₂ is more popular as a

photocatalyst although rutile has been found to be effective under certain specific circumstances (Sherub *et al.*, 2008). In this work, TiO₂ is synthesized into TiO₂ nanoparticles and nanotubes for two different applications. In the following section, the reasons for choosing TiO₂ nanoparticles and nanotubes are discussed.

2.4.2 TiO₂ nanoparticles

Kato *et al.* (1964) studied the photocatalytic oxidation of tetralin using TiO₂ suspension, and this was followed by McLintock (1965). Since then, the photocatalytic properties of TiO₂ have been investigated extensively and have been developed for many successful applications such as the decontamination and the disinfection of water and air (Peral *et al.*, 1997, Crittenden *et al.*, 1997, Gaya and Abdullah, 2008, Swetha *et al.*, 2010b), conversion of water to hydrogen and oxygen (Akira and Kenichi, 1972, Maeda, 2011), and antimicrobial biomedical materials (Monteiro *et al.*, 2009, Rupp *et al.*, 2010, Markowska-Szczupak *et al.*, 2011). The nanoparticles have good electrical, optical and magnetic properties that are different from their bulk counterparts. Various investigations have established that TiO₂ in the form of nanoparticles is more effective as a photocatalyst. The control of the size, shape, and structure of the colloidal precursor is an important factor in determining the properties of the final material. Recently, several techniques have been reported for synthesizing TiO₂ nanoparticles through controlled nucleation and growth processes in dilute Ti (IV) solutions. Among these techniques are the sol-gel, hydrothermal and peptization methods with the advantage of low reaction temperature.

TiO₂ photocatalysts have been investigated extensively for killing or the growth inhibition of bacteria (Fu *et al.*, 2005). Reactive oxygen species (ROS) generated can

oxidize organic compounds on the TiO_2 surface, resulting in the death of microorganisms in the presence of UV light or loading with other metals. Many investigations have reported that the addition of noble metals such as gold and silver may enhance the overall photoefficiency of TiO_2 . However, the selection of the best noble metal and optimizing the content of dopants incorporated into TiO_2 is very important for practical applications. It is believed that loading the optimum amount of cationic dopants could extend the lifetimes of charge carriers and suppress the recombination losses effectively. A variety of noble metal doped TiO_2 have been synthesized to improve the efficiency of the photocatalytic activity of TiO_2 in killing bacteria and this will be discussed in section 2.4.4.

In order to improve the immigration of photo-induced charge carriers, considerable effort has been exerted to improve the antibacterial and cell viability performance under fluorescent light. Ag-TiO_2 nanoparticles have gained much attention and have become a favourite study among researchers. The best properties of Ag-TiO_2 nanoparticles gained from this research primarily depend on the nature of the preparation method and the role optimum Ag content incorporated into TiO_2 . Therefore, in subsequent sections, the basic principle, material selection and the work done by various researchers with regards to TiO_2 , Ag-TiO_2 and other dopants applied in air purification applications will be reviewed. The relationship between Ag on TiO_2 photocatalysis in deactivating bacteria remains unclear, hence the mechanism of the reactions will also be discussed. The toxicity studies of TiO_2 nanoparticles are still a matter of debate especially when the size of the nanoparticles is below 50 nm. Concerning the toxic effects of TiO_2 nanoparticles to human beings, the size of the nanoparticles synthesized by other researchers will also be reviewed.

2.4.3 TiO₂ nanotubes

Particulate TiO₂ film has been used since the discovery of PEC (photo electrochemical water splitting) (Fujishima and Honda, 1972). TiO₂ has been widely used in medical applications (Popat *et al.*, 2007a, Aninwene *et al.*, 2008, Vasilev *et al.*, 2010). TiO₂ with a well-aligned nanotubular structure provides unique electronic properties such as high e⁻ mobility, high specific area, excellent ability to absorb *hν* (photon energy) and high mechanical strength (Roy *et al.*, 2011). It is also light, corrosion resistant, strong and suitable for medical implant applications (Oh and Jin, 2006).

The fluoride-based electrolyte has received great interest because of its controllable, reproducible results as well as the simple process (Kim *et al.*, 2008a). Zwilling *et al.* (1999) first reported on the fabrication of a self-ordered TiO₂ nanotubular structure by anodizing Ti in electrolytes containing fluoride ions. By using nonaqueous electrolytes (ethylene glycol), ultrahigh aspect ratio (length/diameter) nanotubes were achieved. It is well known that the cellular response is strongly affected by the surface morphology. It has also been reported that the natural oxide layer formed on the surface plays a critical role in biocompatibility (Tsuchiya *et al.*, 2006). Studies by Oh *et al.* (2006) have showed that the presence of the TiO₂ nanotube layer significantly accelerates osteoblasts growth and adhesion. TiO₂ also has the capability to inactivate microbial toxins (e.g. lipopolysaccharide endotoxin, brevetoxins, microcystins) and kill a wide range of organisms including bacteria, fungi, algae, viruses and cancer cells in the presence of UV light (Foster *et al.*, 2011).

It is believed that the antimicrobial activities of the TiO₂ nanotubes are highly dependent on the dopant's type. Ag was incorporated into TiO₂ nanotubes and the antimicrobial activities surfaces were investigated. The optimum amount of Ag incorporated into TiO₂ nanotubes is believed to have abundant electron traps so as to be favorable for the separation of the photoinduced electron-hole pairs, which could greatly enhance the activity of the photocatalysts and subsequently kill the microorganisms.

The greatest concerning Ag-TiO₂ as an implant is the toxic effects in medical applications. Some studies have shown that the TiO₂ nanotubes are not toxic both *in vitro* (Feschet-Chassot *et al.*, 2011, Wadhwa *et al.*, 2011) and *in vivo* studies (Popat *et al.*, 2007b). However, some reports showed contradicting results where TiO₂ nanotubes have toxic effects (Peters *et al.*, 2004, Zhang and Sun, 2004). Many physical and chemical factors influence the antibacterial and toxicity effects of TiO₂ nanotubes and it will be discussed in detail. In order to improve the properties of Ti as an implant, the surface modification of Ti will be reviewed.

2.4.4 Modification of TiO₂ to harvest visible light

The photocatalytic capability of TiO₂ is limited to ultraviolet (UV) light (wavelength <400 nm) illumination. The application of TiO₂ is restricted to UV light photoactivation for the generation of highly reactive oxygen species (i.e., hydroxyl radicals). This is an economical and technological limitation for the use of renewable energy sources such as solar light since UV light only accounts for a small portion (3% to 4%) of the whole solar spectrum while visible light accounts for 45% of the solar spectrum (Pelaez *et al.*, 2012a, Khan *et al.*, 2008). This means that only about 3% to 4% of the solar spectrum can be utilized by pure TiO₂. If UV light is the source of radiation,

the photocatalytic process must be conducted in a closed and protected space, which makes it impossible to be processed in open spaces. In response to these deficiencies, many researchers have proposed several attempts to develop and enhance its activity in the visible light region. The effects of the addition of noble metals and ion doping can be beneficial in decreasing the e^- and h^+ pair recombination rate thereby increasing the quantum yield of the photocatalytic process. Doping the semiconductor with a metal and metal ion also enables visible light absorption by providing defect states in the band gap (Subramanian *et al.*, 2003). The mechanism of heterogeneous photocatalysis in the presence of TiO_2 will also be discussed.

2.4.4.1 Noble metal loading

The photocatalytic mechanism is initiated by the absorption of the photon $h\nu_1$ with energy equal to or greater than the band gap of TiO_2 (~ 3.2 eV), producing an electron-hole pair on the surface of TiO_2 nanoparticles as schematized in Figure 2.1. The visible light photoactivity of metal-doped TiO_2 can be explained by a new energy level produced in the band gap of TiO_2 by the dispersion of metal nanoparticles in the TiO_2 matrix. As shown in Figure 2.1, the electron can be excited from the defect state to the conduction band by photons with energy equals to $h\nu_2$. These noble metals act separately or simultaneously depending on the photoreaction conditions and they may: (i) enhance the electron-hole separation by acting as electron traps, (ii) extend the light absorption into the visible range and enhance surface electron excitation by plasmon resonances excited by visible light, and (iii) modify the surface properties of photocatalyst (Sherub *et al.*, 2008). Noble metals that are widely used are Ag, Pt, Au, Pd and Cu. These noble metals have a lower Fermi level than TiO_2 (Sherub *et al.*, 2008).

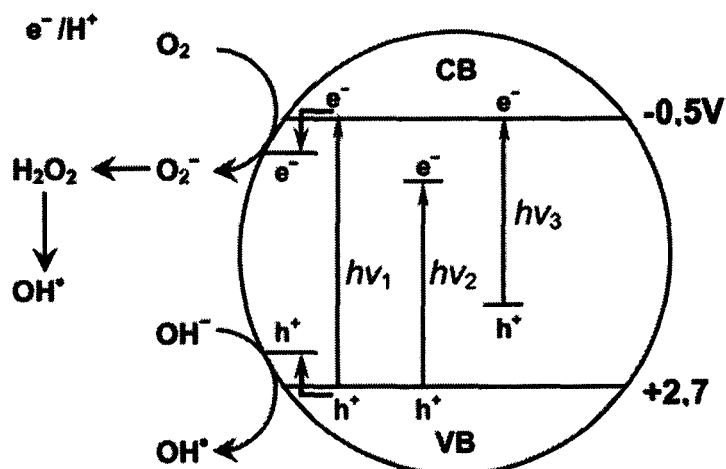


Figure 2.1: Mechanism of TiO₂ photocatalysis: $h\nu_1$: pure TiO₂; $h\nu_2$: metal-doped TiO₂ and $h\nu_3$: nonmetal-doped TiO₂.

The effect of platinum (Pt) doping on TiO₂ is mainly studied for hydrogen generation from water and the degradation of organic pollutants (Kim *et al.*, 2005). Kim *et al.* (2005) successfully demonstrated that the band gap of Pt-TiO₂ is lower than that of undoped TiO₂ by about 0.2 eV. The visible light activity of Pt ion-TiO₂ is strongly affected by the calcination temperature and the concentration of Pt ion dopant which are optimal at 673 K and 0.5 atom %, respectively. Anpo *et al.* (2003) found that Pt loading reduced the amount of Ti³⁺ (evidence of the occurrence of electron transfer from TiO₂ to Pt). Pt traps photogenerated electrons and subsequently increases the photo-induced electron transfer rate at the interface (Anpo and Takeuchi, 2003).

The photocatalytic antimicrobial activity over Cu doped under visible light was reported by Karunakaran *et al.* (2010). 2 % of Cu-doped TiO₂ shifted the optical absorption edge to the visible region but increased the charge-transfer resistance and decreased the capacitance. It was very efficient to disinfect the *E. coli* (Karunakaran *et al.*, 2010). The optimum metal loading was found for 0.5 M % of copper ion to enhance

photoactivity (Colón *et al.*, 2006). The stabilization of the Cu₂O species in doped TiO₂ was due to the preparation of Cu-TiO₂ in the presence of sulphuric acid.

Among the noble metals, Ag is the most preferable noble metal to be loaded into TiO₂ compared to other noble metals because Ag has unique properties as an antimicrobial agent and is applied in a wide range of applications especially in disinfecting medical devices. Ag is well known as non-toxic in spite of claims of killing many different disease organisms. Hence, it is very suitable for indoor air quality applications due to its non-toxic properties. According to the literature, silver is skin friendly and does not cause skin irritations (Klaus-Joerger *et al.*, 2001). Moreover, Ag is more economical than Au and Pt.

Ashkarran *et al.* (2011) carried out synthesis using the sol gel method. It was found that by increasing the silver concentration in the TiO₂ matrix, the antibacterial activity was enhanced remarkably. 0.15 g Ag/TiO₂ nanoparticles exhibit the highest antibacterial activity. The significant enhancement in the antibacterial properties of Ag/TiO₂ nanoparticles under visible light irradiation can be ascribed to the effect of doped noble metal Ag by acting as electron traps in the TiO₂ band gap (Ashkarran *et al.*, 2011). Gunawan *et al.* (2009) reported that the antimicrobial activity increased with higher Ag-TiO₂ loadings from 1 to 500 mg L⁻¹. The reversible photoswitching of nano silver on TiO₂ resulted in excitation and a reverse electron flow from silver to the TiO₂ support, oxidising silver ($\text{Ag}^{\circ} \rightarrow \text{Ag}^{+}$) in the process (Gunawan *et al.*, 2009). However, the toxicity study was not done in this work.

The deactivation of both Gram-positive (*S. aureus*) and Gram-negative (*P. aeruginosa*, *E. coli*) bacteria with Ag-doped TiO₂ nanoparticles (3% and 7%) was reported by Gupta *et al.* (2013). The viability of all three microorganisms was reduced to zero at 60 mg/30 mL culture in the case of both (3% and 7% doping) concentrations of Ag-doped TiO₂ nanoparticles. Annealed TiO₂ showed zero viability at 80 mg/30 mL whereas doped Ag-TiO₂ 7% showed zero viability at 40 mg/30 mL culture in the case of *P. aeruginosa* only (Gupta *et al.*, 2013). In this work, antibacterial activity was focused but the toxicity study was not reported.

Ag-TiO₂ nanoparticles are prepared with the sol-gel method using a reduction agent as reported by Lee *et al.* (2005). When the AgNO₃ content is 2 mmol/mol of TiO₂, the major phase (111) of silver could be clearly seen. 70% of p-nitrophenol is degraded after 60 minutes of UV irradiation for TiO₂. In the case of Ag-TiO₂, 90% of p-nitrophenol is degraded. The improvement in the photocatalytic activity is related to the transportation of electrons from the TiO₂ conduction band to the Ag particles (Lee *et al.*, 2005). In this work, antimicrobial activity is not reported.

Almost all studies only reported on the antimicrobial study of Ag-TiO₂, but very few on the toxicity effects. In completing this work, the detailed work of Ag-TiO₂ nanoparticles and nanotubes were studied in turning the photocatalytic of TiO₂ into the visible light region. Physical properties, antibacterial study, the mechanism of cell wall decomposition and toxicity effects were studied for TiO₂ nanoparticles and nanotubes.

2.4.4.2 Metal ion loading

Transitional metals are either deposited or doped on the TiO₂ surfaces as metallic nanoparticles are doped as ionic dopants. The doping elements are usually Cr, Fe, V, Nb, Sb, Sn, P, Si, Al and Zr. Figure 2.2 shows the effect of different metals in TiO₂ to absorb visible light and to enhance photocatalytic activity. Some doping has the possibility to inactivate microorganisms under visible light irradiation. More details of the cation doping TiO₂ are shown in Table 2.2. The replacement of cationic ions within the crystal lattice may create impurity energy levels that facilitate better absorption in the visible light region as depicted in Figure 2.2.

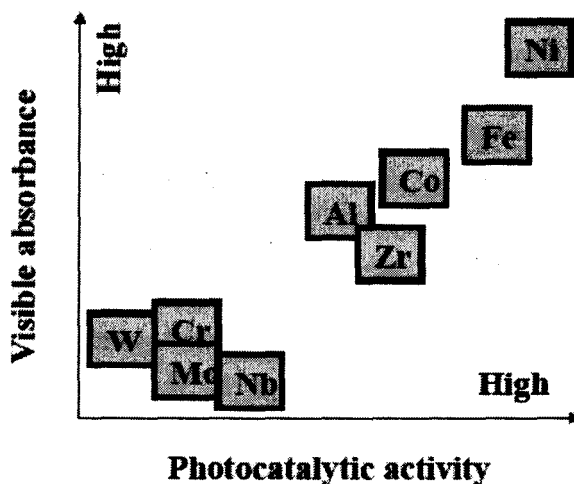


Figure 2.2: Effect of cationic doping compounds in terms of visible light absorbance and photocatalytic activity (Hwang *et al.*, 2006, Yanjun *et al.*, 2006).

Luu *et al.* (2010) synthesized Fe-doped into TiO₂ by the sol gel method. Fe-doped TiO₂ enabled the photon absorbing zone of TiO₂ to extend from UV towards the visible waves as well as to reduce its band gap energy from 3.2 to 2.67 eV. The photocatalytic activities of the TiO₂ samples modified by Fe³⁺ have been found to be higher than those of pure TiO₂ by about 2.5 times (Luu *et al.*, 2010). Fe ions trap not only electrons but also holes which lead to the increase of photoactivity (Litter, 1999,

Jiefang *et al.*, 2003). The maximum photoactivity appears with 0.5 wt % of Fe^{3+} due to the decrease in the density of the surface active centers (Chatterjee and Dasgupta, 2005). According to George *et al.* (2011), the photo-oxidation capability of Fe-doped TiO_2 is found to increase during near-visible light exposure. The cytotoxic and ROS production shows the increasing of oxidant injury and the cell death of a macrophage cell line with a decrease in the band gap energy (George *et al.*, 2011).

Tsai *et al.* (2012) reported that the absorption spectra of the nanoparticles shift towards the visible light regions depending on the Al_2O_3 addition. Ti^{4+} and Ti^{3+} coexist in the synthesized Al-doped TiO_2 . The Ti^{3+} concentration however increases with the increasing of Al_2O_3 addition due to Al/Ti substitution that causes the occurrence of oxygen vacancy (Tsai *et al.*, 2012). Aluminium doping is used on TiO_2 for a potential application in thermal shock due to its stable thermal expansion coefficient and physical property (Li *et al.*, 2006). The presence of metal dopants effectively increases the photocatalytic activity of TiO_2 thin films in the following order: $\text{Ag/TiO}_2 > \text{Zr/TiO}_2 > \text{Fe/TiO}_2 > \text{TiO}_2$ (Kment *et al.*, 2010).

Another alternative to metal ions is Zr ions, which is rarely reviewed. Liu *et al.* (2009) synthesized Zr-doped TiO_2 nanotube arrays by the electrochemical method. Zr/TiO_2 nanotube arrays doped at 7 V and calcined at 600 °C achieved the best photocatalytic efficiency and the most optimal doping ratio was 0.047 (Zr/Ti). The increase in photocatalytic activity was due to the increased number of oxygen vacancies. Zr incorporated into the TiO_2 lattice and induced a relatively larger lattice strain. (Liu *et al.*, 2009). However, the photocatalytic test was only performed under UV light and no antimicrobial activity was done in this work.

According to Swetha *et al.* (2010), Zr-doped TiO₂ at the molecular scale exhibited better photocatalytic activity with a lower bandgap energy. The work reported that the optical absorption edge shifted slightly from 400 nm to about 450 nm. Zr-doped TiO₂ can inactivate *P. aeruginosa* by 100% within 150 minutes of exposure. (Swetha *et al.*, 2010a). However, the photocatalytic and antibacterial activity were done only under sunlight. The toxicity study was also not reported.

Stengl *et al.* (2008) found that doping Zr-TiO₂ prepared by the homogeneous hydrolysis of titanium and zirconium oxo-sulphates mixture in aqueous solutions have a positive influence on the degradation activity of warfare agents and decreases the photocatalytic degradation of Orange 2 dye. The presence of Zr⁴⁺ dopant increases the surface area, crystallites size and accelerates the surface hydroxylation. Total degradation soman (3,3-dimethyl-2-butyl methylphosphonofluoridate or GD) and matter VX (O-ethyl S-2-(diisopropylamino)ethyl methylphosphonothionate) on Zr-doped titania run up through 1 minute is for a sample with ~13.2 weight % Zr (Štengl *et al.*, 2008). In this work, antibacterial and toxicity activities were not done.

Moafi *et al.* (2011) found that Ag-Zr co-doped TiO₂ nanoparticles has a more significant efficiency in photocatalytic activity compared to Ag-TiO₂ and Zr-TiO₂. However, this paper only reported on the photocatalytic test but did not test on the antibacterial and toxicity studies. Moreover, the research did not study the different compositions of Zr. In this study, different compositions of Ag-Zr were studied and the results were compared with TiO₂, Ag-TiO₂ and Zr-TiO₂ in terms of physical properties, antibacterial and toxicity study to complete the set.

2.5 Photocatalytic inactivation of microorganism

Photocatalysis is the acceleration of a photoreaction in the presence of a catalyst. In 1972, Fujishima and Honda discovered that water molecules were splitted using TiO₂ electrodes under ultraviolet (UV) irradiation (Fujishima and Honda, 1972). The underlying mechanism of TiO₂ photocatalysis is the light-induced generation of electron-hole pairs in a crystalline form of TiO₂. The principles of semiconductor-based photocatalysis can be schematically demonstrated in Figure 2.3 (Linsebigler *et al.*, 1995, Haghghi *et al.*, 2011, Cho *et al.*, 2004). Upon irradiation with photons less than 380 nm, electrons in the valence band were excited to the conduction band and formed electrons (e_{cb}^-) and holes (h_{vb}^+) on the surface of nanoparticles as shown in equation (2.1), and electron-hole pairs were created on the surface of the photocatalyst (Kartsonakis *et al.*, 2008). This stage is referred as the semiconductor's 'photo-excitation' state (Maness *et al.*, 1999). Oxygen acted as an electron acceptor by forming a superoxide radical anion ($O_2^{\bullet-}$), strong oxidative radicals that can decompose organic compounds (Miao *et al.*, 2004, Kangwansupamonkon *et al.*, 2009) as shown in equation (2.2). Holes could react with water adhering to the surfaces of semiconductor particles to form hydroxyl radical (OH^\bullet) as shown in equation (2.3) (Maness *et al.*, 1999). In the literature, OH^\bullet , HO_2^\bullet , H_2O_2 are considered to be the key reactive oxygen species (ROS) generated in the photocatalytic reaction (Liou and Chang, 2012). These electrons and holes attacked the organic compounds producing less harmful and nontoxic products as shown in equation (2.4). In this work, the mechanisms of Ag-TiO₂ will be discussed in detail in Chapter 4 based on the SEM and TEM observations.

